Biointerface Research in Applied Chemistry
Platinum Open Access Journal (ISSN: 2069-5837)

Article
Volume 11, Issue 3, 2021, 9880 - 9903
https://doi.org/10.33263/BRIAC113.98809903

Structural Study and Vibrational Assignments of Anticonvulsant Topiramate by using DFT calculations and Two Harmonic Force Fields

José Ruiz Hidalgo [1], Silvia Antonia Brandán [1,*]

[1] Cátedra de Química General, Instituto de Química Inorgánica, Facultad de Bioquímica, Química y Farmacia, Universidad Nacional de Tucumán, Ayacucho 471, 4000, San Miguel de Tucumán, Tucumán, Argentina
* Correspondence: silvia.brandan@fbqf.unt.edu.ar;

Scopus Author ID 6602262428
Received: 1.09.2020; Revised: 19.09.2020; Accepted: 19.09.2020; Published: 22.09.2020

Abstract: B3LYP/6-311++G** calculations have been combined with the scaled quantum mechanical force field (SQMFF) methodology to study structural and vibrational properties of anticonvulsant topiramate (TPM) agent. The 123 vibration modes expected for TPM were completely assigned, considering two harmonic force fields. In one case, C_{2V} symmetries were considered for both SO_2 and NH_2 groups, while in the other one C_{2V} and C_{3V} symmetries for the NH_2 and SO_3 groups, respectively. The calculated harmonic vibrational frequencies are consistent with the experimental IR and Raman spectra in the solid phase. Very good concordances were found between the theoretical structures in gas phase and aqueous solution and the corresponding experimental reported. Thus, the fused five-membered ring in TPM produces that the pyranose ring adopts distorted twist-boat conformation, as was experimentally observed. In solution, all calculations were performed with the self-consistent reaction force (SCRF) method by the integral equation formalism variant polarised continuum (IEFPCM) and universal solvation model density (SMD) models. The corrected solvation energy value for TPM in aqueous solution by total non-electrostatic terms and by ZPVE is -1066.10 kJ/mol. The bond orders have evidenced that the three O atoms are not linked of the same form to S atom. Hence, the S atom of TPM is practically tetra-coordinate in both media, as evidenced by the high negative MK and NPA charges on the O atoms linked to it. The AIM study supports the higher stability of TPM in the gas phase while the NBO calculations suggest higher stability in solution. Gap values support the higher reactivity of TPM in solution than in the gas phase. The scaled force constant for both cases are reported for the first time. Comparisons of predicted ^{1}H- and ^{13}C-NMR spectra with the corresponding experimental ones reveal very good concordances.

Keywords: Topiramate; molecular structure; DFT calculations; vibrational spectra.

1. Introduction

Topiramate (TPM) is a sulfamate monosaccharide used to treatment of epilepsy due to its anticonvulsant and antiepileptic properties [1-7]. The experimental structure of TPM was determined by Kubicki *et al*. [1], while its vibrational characterization by means of the infrared and Raman spectra and thermal properties were reported by Sena *et al*. [4]. These authors have optimized the structure in the gas phase with the B3LYP/6-31G* method using the Gaussian 98 package, while the tentative vibrational assignments only for some vibration modes were based on published assignments for sulfamates, other correlated materials, and DFT calculations. In that work, some vibration modes corresponding to the SO_3 group were no

descript correctly because they have considered C_{3v} symmetry for that group but have assigned three symmetric and only one antisymmetric SO_3 modes instead of two antisymmetric and one symmetric SO_3 modes. Moreover, for the NH_2 group, they have reported only the antisymmetric and symmetric stretching modes while the deformation, wagging, rocking, and twisting modes expected for this group have not been reported yet. Hence, to identify TPM in all media by using vibrational spectroscopy, it is necessary to correct and complete assignments of all observed bands in the infrared and Raman spectra to the normal vibration modes. In this work, the TPM structure was optimized in the gas phase and in aqueous solution with the B3LYP/6-311++G** level of theory [8,9] and the Gaussian 09 program [10] while the complete vibrational assignments of TPM were performed combining the normal internal coordinates and the scaled quantum mechanical force fields (SQMFF) methodology with transferable scaling factors and the Molvib program [11-13]. Hence, the complete assignments of 123 vibration modes of TPM in the gas phase were proposed with the B3LYP/6-311++G** level of theory and by using two harmonic force fields. Hence, the normal internal coordinates of the sulfamate group (O-SO_2-NH_2) of TPM have been defined of two forms: in one case, both SO_2 and NH_2 groups were considered with C_{2V} symmetries, and, in the other one, the NH_2 and SO_3 groups present C_{2V} and C_{3V} symmetries, respectively. Here, the scaled force constants for those two different force fields obtained for TPM in both media were also reported. Besides, the structural, electronic, and topological properties were also reported in the gas phase and aqueous solution at the same level of theory. The calculations in aqueous solution were carried out with the self-consistent reaction force (SCRF) method and the integral equation formalism variant polarised continuum model (IEFPCM) method and universal solvation model density (SMD) models [14-16]. In addition, reactivities and behaviors of TPM in both media were predicted by using the frontier orbitals and some important descriptors [17-21]. Here, the predicted infrared, Raman, ^{1}H-, ^{13}C-NMR, and ultraviolet-visible spectra were compared with the corresponding available ones [7,22].

2. Materials and Methods

The experimental CIF file determined for TPM by using X-ray diffraction was used as an initial theoretical structure and, then, the optimizations of it in the gas phase and aqueous solution were performed with the Gaussian 09 program [10] and the B3LYP/6-311++G** level of theory [8,9]. All calculations in solution were carried out with the self-consistent reaction force (SCRF) method by the integral equation formalism variant polarised continuum (IEFPCM) and universal solvation model density (SMD) models [14-16]. A scheme of the structure of TPM showing all groups present can be seen in Figure 1 together with the definition of three rings. R1 is the six members' ring, while R2 and R3 are the five member's rings. Note that R2 and R3 rings have every two CH_3 groups. In the vibrational analyses, two harmonic force fields were considered because the normal internal coordinates were built using two forms to define the normal internal coordinates of sulfamate group (O-SO_2-NH_2), one form is to consider C_{2V} symmetries for both SO_2 and NH_2 groups and, the other one, to consider C_{2V} and C_{3V} symmetries for the NH_2 and SO_3 groups, respectively. Besides, each pair of methyl groups was considered with C_{2V} symmetry. After that, transferable scaling factors together with each set of normal internal coordinates were used with the scaled quantum mechanical force fields (SQMFF) methodology and the Molvib program to perform the complete vibrational assignments of TPM [11-13]. Here, in the assignments of the bands observed in both infrared

and Raman spectra to the normal vibration modes, potential energy distribution (PED) contributions ≥ 10 % were considered.

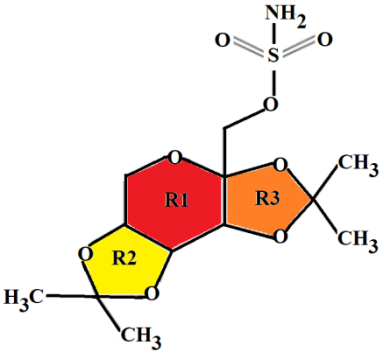

Figure 1. Schematic structure of TPM together with the definition of three rings in different colors.

The Raman spectrum predicted in activities was corrected to intensities by using known equations [23,24]. Structural, electronic, topological, and vibrational properties were evaluated in both media and at the same level of theory. Hence, atomic charges, stabilization energies, molecular electrostatic potentials, bond orders, and topological properties were investigated in both media by using the Merz-Kollman (MK) scheme and natural bond orbital (NBO) and atoms in molecules (AIM) calculations [25-28]. The mapped MEP surfaces were obtained with the *GaussView* program [29], while the volume variation was calculated with the Moldraw program [30]. Energy gap values were calculated from the differences between both frontier orbitals while the chemical potential (μ), electronegativity (χ), global hardness (η), global softness (S), global electrophilicity index (ω), and global nucleophilicity index (E) descriptors were calculated with the gap values [17-21]. The ultraviolet-Visible and ^{1}H and ^{13}C NMR spectra were predicted in aqueous solution by using the Time-dependent DFT calculations (TD-DFT) and the gauge-including atomic orbital (GIAO) method at the same level of theory [31].

3. Results and Discussion

3.1. Geometrical parameters and properties in both media.

The optimized structure of TPM in the gas phase with the atoms labeling is presented in Figure 2 together with the definition of three rings in different colors while in Table 1 can be observed the energy values, dipole moments, and volumes calculated for TPM in both media by using the B3LYP/6-311++G** level of theory. Note that the E corrections by zero-point vibrational energy (ZPVE) are also presented in the table. With (1) are expressed the uncorrected E values while the corrected ones by ZPVE are identified as (2). In solution, the dipole moment value is higher, as compared with the value in the gas phase because the structure is hydrated with water molecules in this medium, and, for this reason, a slight increase in the volume is also observed, as a consequence of the hydration. The biological properties of TPM can be attributed to donors and acceptors groups of H bonds; thus, in its structure, there are two donors N-H bonds (NH_2 group) and nine acceptors H bonds (N and O atoms). Khalil *et al*. reported that the solubility of TPM in water is 9.8 mg/mL; however, it is most soluble in alkaline solutions with a pH of 9–10 [7]. Hence, the presence of those donors and acceptors groups justify the solubility of TPM in water, and probably a high solvation energy value is expected for TPM in aqueous solution. Taking into account that TPM is very sensitive to water

and should therefore be well protected from moisture [7], its corrected solvation energy (ΔG_c) is predicted in aqueous solution by using the B3LYP/6-311++g(d,p) method. Figure S1 shows few changes in the orientations and directions of dipole moment vectors predicted for topiramate in both media by using the B3LYP/6-311++G** level of theory.

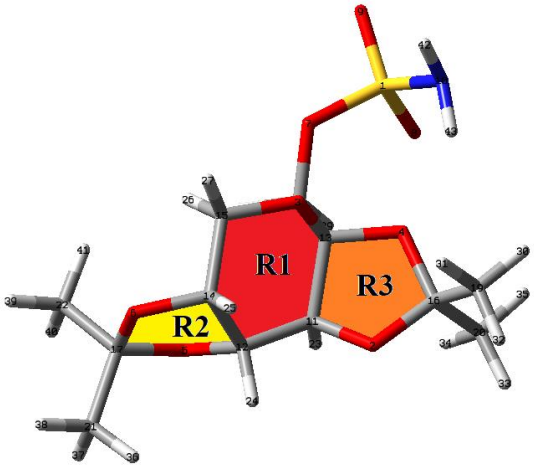

Figure 2. Optimized structure of TPM with the atoms labeling together with the definition of three rings.

Table 1. Calculated total energies (*E*), dipole moments (μ), and volumes (V) of TPM in the gas phase and aqueous solution by using the B3LYP/6-311++g(d,p) method.

B3LYP/6-311++g(d,p) method					
Medium	(1) E (Hartrees)	(2) E_{ZPVE}	μ (D)	V (Å^3)	ΔV
TPM					
GAS	-1524.5685	-1524.2170	6.82	318.3	1.1
PCM/Water	-1524.9606	-1524.6139	8.62	319.4	

Hence, Table 2 is given the corrected ΔG_c values calculated from the difference between the values in solution and in the gas phase. Note that the corrected value by total non-electrostatic terms and by ZPVE (-1066.10 kJ/mol) is slightly higher than the uncorrected by ZPVE (-1053.51 kJ/mol).

Table 2. Corrected and uncorrected solvation energies (ΔG_{un}) by the total non-electrostatic terms (ΔG_{ne}) and by zero-point vibrational energy (ZPVE) of TPM in aqueous solution by using the B3LYP/6-311++g(d,p) method.

B3LYP/6-311++G(d,p) Method[a]			
Solvation energy (kJ/mol)			
Medium	ΔG_{un}[#]	ΔG_{ne}	ΔG_c
PCM/Water (2)	-1041.06	25.04	-1066.10
PCM/Water (1)	-1028.47	25.04	-1053.51

But, both values of TPM are higher than the observed for some salts with antiviral properties such as foscarnet (-219.64 kJ/mol) or brincidofovir (-227.34 kJ/mol) [32,33] or, for some cationic species of alkaloids as, heroin (-323.14 kJ/mol) or scopolamine (-310.34 kJ/mol) [34,35]. Table 3 shows that the total acceptors and donor groups of TPM cannot justify the high solvation energy because it has a total of 11 groups against foscarnet, which presents 19 groups. Moreover, although those values of compared species were calculated with the B3LYP/6-31G* method, the different methods used cannot explain the great difference in the solvation energy value of TPM. Evidently, the presence of the sulfamate group (O-SO_2-NH_2) and, in particular, of SO_3 group in TPM, is essential to validate that high solvation energy value in aqueous solution.

Table 3. Uncorrected solvation energies by ZPVE energies (ΔG_C) and numbers of N-H and O-H groups and N and O atoms present in TPM and in antiviral and alkaloids species in aqueous solution by using the hybrid B3LYP/6-311++G** and B3LYP/6-31G* methods.

Nº	Species	ΔG_C	N-H	O-H	O	C=O	N	Total	Groups	Rings
1	TPM[a]	-1053.51	2(NH_2)		8		1	11	O-SO_2	2R5,R6
2	Foscarnet[b]	-219.64		12	5	2		19	3 Na, PO_3	
3	Brincidofovir[c]	-227.34	2(NH_2)	2	7	1	3	15	HPO_3	R6
4	Heroin[d]	-323.14	1		5	2	1	9		R5,4R6
5	Scopolamine[e]	-310.34	1	1	4	1	4	11	1R3	2R6,R5

[a]This work, [b]From Ref [32], [c]From Ref [33], [d]From Ref [34], [e]From Ref [35]

Comparisons of calculated geometrical parameters of TPM in both media with the corresponding experimental ones determined by Kubicki *et al*. by X-ray diffraction can be seen in Table 4 as a function of root-mean-square deviation (RMSD) values.

Table 4. Comparisons of calculated geometrical parameters of TPM in the gas phase and aqueous solution by using the B3LYP/6-311++G** method with the corresponding experimental ones by means of the of root-mean-square deviation (RMSD) values.

Parameters	B3LYP/6-311++G** method[a]		Experimental[b]
	Gas	Water	
Bond lengths (Å)			
S1-N10	1.66	1.64	1.58
S1-O8	1.45	1.45	1.42
S1-O9	1.44	1.45	1.42
S1-O7	1.66	1.63	1.58
O7-C18	1.43	1.45	1.44
C18-C13	1.54	1.52	1.51
C13-O4	1.40	1.40	1.41
C13-O3	1.42	1.42	1.41
C13-C11	1.54	1.54	1.53
O4-C16	1.45	1.46	1.44
C16-C19	1.52	1.51	1.50
C16-C20	1.52	1.52	1.51
C16-O2	1.42	1.49	1.42
O2-C11	1.42	1.42	1.42
C11-C12	1.52	1.52	1.51
C12-C14	1.53	1.53	1.54
C12-O5	1.42	1.43	1.41
C14-C15	1.53	1.52	1.50
C14-O6	1.42	1.43	1.43
C15-O3	1.42	1.43	1.42
O5-C17	1.43	1.43	1.42
O6-C17	1.44	1.45	1.42
C17-C21	1.52	1.52	1.48
C17-C22	1.52	1.51	1.51
RMSD[b]	**0.029**	**0.027**	
N10-S1-O7	105.8	108.4	99.9
N10-S1-O8	107.4	108.1	108.9
N10-S1-O9	107.8	107.6	111.6
O8-S1-O9	123.6	120.5	119.0
O8-S1-O7	107.8	103.4	115.6
O9-S1-O7	103.1	108.4	107.3
S1-O7-C18	118.6	121.2	115.6
O7-C18-C13	113.5	112.0	110.4
C18-C13-C11	112.9	113.0	117.1
C18-C13-O3	110.3	112.3	113.6
C18-C13-O4	112.8	109.6	110.3
C13-O4-C16	109.4	110.6	110.3
O3-C13-O4	106.3	106.0	110.7
C13-O3-C15	114.2	114.7	114.1

Parameters	B3LYP/6-311++G** method[a]		Experimental[b]
	Gas	Water	
Bond lengths (Å)			
C13-C11-O2	102.4	101.8	103.3
C13-C11-C12	115.8	116.7	114.3
O4-C16-O2	105.3	104.1	104.5
O4-C16-C19	110.4	109.8	108.8
O4-C16-C20	107.5	108.4	109.8
C16-O2-C11	108.9	108.2	106.6
C19-C16-C20	113.9	113.6	113.0
C19-C16-O2	108.5	109.0	109.0
C20-C16-O2	110.9	111.5	111.4
O2-C11-C12	108.3	108.1	107.4
C11-C12-C14	116.3	116.3	114.1
C12-C14-C15	111.8	112.2	112.2
C14-C15-O3	110.6	110.3	110.6
C11-C12-O5	109.4	109.6	108.5
C12-O5-C17	106.5	107.3	107.0
C12-C14-O6	103.0	102.9	104
O6-C14-C15	110.5	110.2	108.8
C14-O6-C17	108.9	109.4	109.0
O6-C17-C21	108.4	108.6	109.3
O6-C17-C22	110.4	110.3	109.2
O5-C17-C21	110.9	111.0	111.0
O5-C17-C22	108.5	108.5	109.0
O5-C17-O6	105.8	105.0	103.9
C21-C17-C22	112.7	113.2	114.0
RMSD[b]	**2.62**	**3.00**	
N10-S1-O7-C18	-81.45	-88.31	-165.7
O8-S1-O7-C18	33.24	28.79	-49.1
O9-S1-O7-C18	165.44	157.67	80.5
O7-C18-C13-O3	34.35	49.10	-179.3
O7-C18-C13-C11	162.0	176.98	-54.7
O7-C18-C13-O4	-84.29	-68.42	63.3

[a]This work, [b]Ref [1]

Note that the RMSD values are presented only for the bond lengths and angles because the higher deviations are observed in the dihedral angles due to that the calculations predict these parameters with different signs and values than the experimental ones, as can be seen in Table 4. Hence, better correlations are observed for bond lengths and angles (0.029-0.027 Å and 3.00-2.62 º) despite the calculated values that are, in general, overestimated. In TPM, the fused five-membered ring produces that the pyranose ring adopts distorted twist-boat conformation, as was experimentally observed [1]. A very important result is observed in the calculated N10-O3 distance between the N atom and the O3 pyranose ring oxygen atom because the calculated values in the gas phase and aqueous solution are respectively of 3.349 and 3.867 Å while the experimental value is 5.965 Å. This N10-O3 distance is probably related to the biological activity of TPM because it connects the hydrophilic part with the corresponding hydrophobic one. These structural results have shown that the B3LYP/6-311++g(d,p) method generates a very good structure to perform the vibrational study by using the normal internal coordinates analysis.

3.2. Atomic charges, molecular electrostatic potentials (MEP), and bond orders (BO) studies.

The above studies have evidenced that the (O-SO_2-NH_2) sulfamate group plays an important role in the structural properties of TPM in both media and, probably, in its pharmacological properties and, in particular, it could have an influence on the high solvation energy value in aqueous solution. Hence, the atomic charges on the atoms of that group should

be first compared with the corresponding to other O atoms of rings and, then, analyzed among them in order to determine the grade of influence of charges on the properties. This way, atomic Merz-Kollman (MK) [28], Mulliken, and natural population atomic (NPA) charges were calculated on all atoms of TPM in the gas phase, and aqueous solution by using the B3LYP/6-311++G** method and the results are presented in Table S1 of supporting material. The variations of those three types of charges only for the S, O, and N atoms of TPM in both media can be seen in Figure 3. This figure shows that the three charges on S1 atom in both media present high positive signs while the MK and NPA charges on the O and N atoms have negative signs.

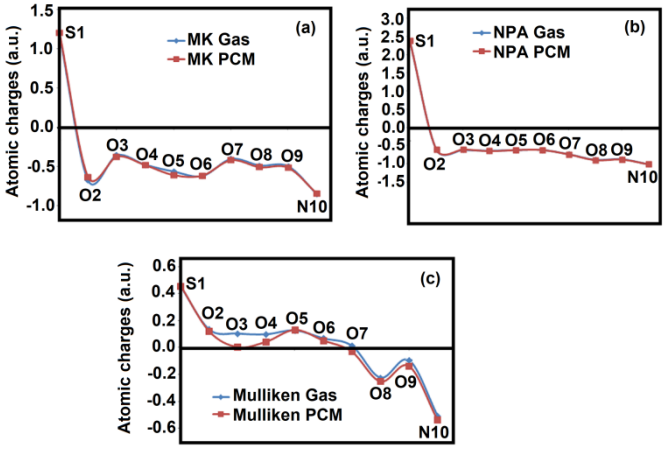

Figure 3. Variations in the atomic Merz-Kollman (MK), Mulliken, and natural population atomic (NPA) charges of TPM in the gas phase and aqueous solution by using the hybrid B3LYP/6-311++G** method.

On the contrary, the Mulliken charges on O8, O9, and N10 present negative signs in both media, while the corresponding to O2, O3, O4, O5, and O6 atoms present positive signs. Note that only the different signs of Mulliken charges on N10 and O3 atoms could explain the shortening in the calculated N10-O3 distance in the gas phase and aqueous solution (3.349 and 3.867 Å), as compared with the experimental value (5.965 Å). On the other side, the three O atoms that belong to the sulfamate group (O7, O8, O9) present practically the same MK and NPA charges while the Mulliken charges on O8 is most negative than the observed on O9 and O7 atoms. Besides, O7 shows a positive sign in the gas phase and a negative sign in solution. Thus, the Mulliken charges on three O atoms of the O-SO_2-NH_2 group will explain the differences between the properties in the gas phase and in solution. In relation to the H atoms, it is observed that the two H42 and H43 atoms that belong to the NH_2 group present the highest positive values than the other ones.

If now the molecular electrostatic potentials (MEP) values are analyzed on all atoms from Table S1, we observed that the values change a little in solution evidencing the most negative value on the S atom while the less negative values are observed on the H atoms, following, in general, the tendency: S > O > N > C > H. However, when the mapped MEP surface for TPM in the gas phase by using the B3LYP/6-31G* method is graphed and presented in Figure 4 as transparent and solid mapped MEP surfaces, the different colorations clearly reveal which are the main reaction sites. Hence, in the two mapped MEP surfaces of Figure 4a and 4b can be seen the strong red colors on the O atoms of O-SO_2- of sulfamate group while the intense blue colors on the H atoms of the NH_2 group.

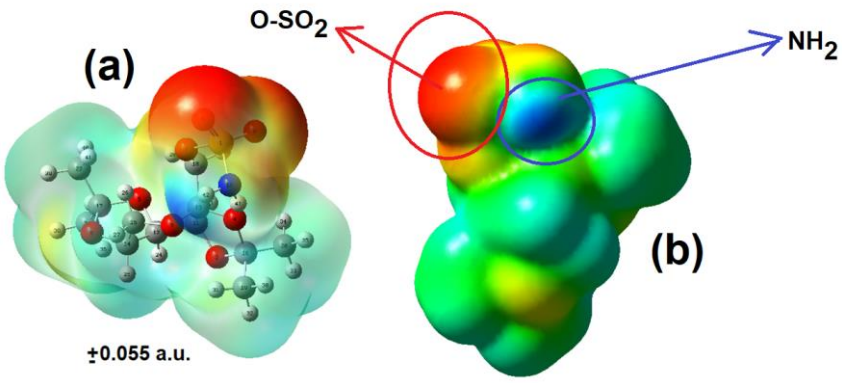

Figure 4. The calculated electrostatic potential surface on the molecular surface of TPM in the gas phase (± 0.055 a.u.). B3LYP functional and 6-31G* basis set. Isodensity value of 0.005.

Note that other regions with orange and light blue colors are also observed on the O atoms of rings and on the H atoms of CH_3 groups, respectively. Thus, the red and blue colors, respectively, are attributed to acceptors and donors H bonds regions, which are known as nucleophilic and electrophilic sites, while the green colors are inert sites. These results are in agreement with that experimental determined by X-ray because the NH_2 group acts as a donor for two intermolecular hydrogen bonds, which are formed with the sulfamate O8 oxygen atom and with the O6 atom of two neighboring molecules [1].

The bond orders (BOs), expressed as Wiberg indexes, are also studied for TPM in both media, which are calculated as totals by atom by using the B3LYP/6-311++G** method and these are presented in Table S1 [25]. Analyzing the BOs only for the ten first atoms, it is observed that the S and N atoms present the higher values while the lowers values are observed for the O8 and O9 atoms of O-SO_2- of sulfamate group. Later, the low BOs values observed in those two atoms could indicate that those two atoms are more acceptors of H bonds than those belonging to rings (most negative charges), as expected because these sites are nucleophilic regions with strong red colors on the mapped MEP surfaces. However, when the Wiberg bond index matrix in the NAO basis is considered for the S1 and O7, O8, and O9 atoms of O-SO_2- group, the values are respectively of 0.6847, 1.3236, and 1.3481, indicating that the three atoms are not linked of the same form to S atom. The BO of S1 atom linked to N10 atom is 0.8912, a value slightly higher than the observed for the O7 atom. The sum of all those values is 4.2476, a value approximately similar than observed for S1 atom in Table S1 (4.2805). In TPM, the S atom is practically tetra-coordinate in both media, as evidenced by the high negative MK and NPA charges on the O atoms linked to it.

3.3. Natural bond orbital (NBO) and atoms in molecules (AIM) studies.

The NBO program allows the determination of bond orders, NPA charges, Natural atomic orbital occupancies, and to perform the Second Order Perturbation Theory Analysis of Fock Matrix in NBO Basis necessary to investigate donor-acceptor energy interactions among other properties [25]. On the other hand, the AIM 2000 program based in the Bader' theory of atoms in molecules (AIM) is useful to predict different types of interactions as for example, intra-molecular or H bonds interactions by means of the topological properties [26,27]. Hence, those two programs were used to determine the main delocalization energies of TPM in the gas phase and aqueous solution by using the B3LYP/6-311++G** method, which is presented in Table S2. The exhaustive inspections of results show that only three interactions are observed

in TPM in both media which are: $\sigma \rightarrow \sigma^*$, $n \rightarrow \sigma^*$ and $\sigma^* \rightarrow \sigma^*$ interactions where the total energy of $n \rightarrow \sigma^*$ interactions show the higher values. These latter interactions are performed from lone pairs of O and N atoms to different antibonding $\sigma O\text{-}C$, $\sigma C\text{-}H$, $\sigma C\text{-}C$, $\sigma S\text{-}O$ and $\sigma S\text{-}N$ orbitals while the $\sigma^* \rightarrow \sigma^*$ interactions are performed from antibonding *S1-O7* orbitals to antibonding $\sigma S1\text{-}N10$ and $\sigma O7\text{-}C18$ orbitals. The total sum of energies favors slightly to TPM in solution with a value of 1688.81 kJ/mol, while in the gas phase, the value is 1656.11 kJ/mol.

Intra-molecular and H bonds interactions for TPM in both media were predicted with the topological properties by using the AIM 2000 program [26,27]. Thus, the electron density distribution, $\rho(r)$, the Laplacian values, $\nabla^2\rho(r)$, the eigenvalues $(\lambda 1, \lambda 2, \lambda 3)$ of the Hessian matrix and the $\lambda 1/\lambda 3$ ratios were calculated in the bond critical points (BCPs) and in the ring critical points (RCPs). These properties in the gas phase and aqueous solution are presented in Tables S3 and S4, respectively. The values of $\lambda 1/\lambda 3 < 1$ and $\nabla^2\rho(r) > 0$ indicate that three H bonds interactions are observed in the gas phase, while in solution, only two H bonds interactions. Hence, in the gas phase are observed the H bonds interactions: N10-H43···O4, C18-H28···O5, and C15-H26···H41 while in solution only are observed two of them: N10-H43···O4 and C15-H26···H41. Note that the formation of an H bond implies the formation of a new RCP named RCPN; hence, three new RCPN are formed in the gas phase (RCPN1, RCPN2, and RCPN3) and only two new RCPN in solution. Obviously, the three rings give three RCP1, RCP2, and RCP3. Figure S2 can be seen in the three H bonds interactions of TPM in the gas phase and the new three RCPN and RCPs. This AIM study supports the higher stability of TPM in the gas phase while the NBO study suggests higher stability in solution.

3.4. Frontier orbitals studies and global quantum descriptors.

Biological studies have suggested that TPM has multiple probable sites of action, including sodium channels, GABA receptors, and glutamate (AMPA) [36], which will explain why TPM is efficient in numerous intractable syndromic epilepsies. These different sites of action are also evidenced by the different colorations on its mapped MEP surface. Then, the studies of frontier orbitals and knowledge of gap energies in different media are parameters very important to predict the reactivities and behaviors of TPM in the gas phase and aqueous solution. Hence, the HOMO and LUMO, energy band gaps and the chemical potential (μ), electronegativity (χ), global hardness (η), global softness (S), global electrophilicity (ω), and nucleophilicity indexes (E) descriptors were calculated for TPM in both media by using the hybrid B3LYP/6-311++G** method. These parameters in both media are compared in Table S5 with the corresponding to the free bases of scopolamine and promethazine by using the B3LYP/6-31G* method [35,37]. The equations used to compute the descriptors can also be seen in the same table. First, it is observed that TPM is slightly most reactive in solution because its gap value in this medium is a few lower than the value in the gas phase. However, when the gap values for the three species are compared, we observed that the species of antihistaminic promethazine agents present in both media the lower gap values, later the free base of scopolamine and, finally, the higher gap values are observed for topiramate. Taking into account that the lower gap value is related to the most reactive species, the reactivity order is promethazine (4.7157/4.7702 eV) > scopolamine (5.4004/5.4758 eV) > topiramate (6.9434/6.9316 eV). If now the global electrophilicity (ω) and nucleophilicity indexes (E) are compared, the tendency in both indexes change to: topiramate (ω: 2.3503/2.3507, E: -14.025/-13.990 eV) > scopolamine (ω: 1.7393/1.7504, E: -8.2756/-8.4763 eV) > promethazine (ω:

1.4911/1.4954, *E*: -6.2524/-6.3701 eV). These high values of both ω and *E* indexes for topiramate could probably explain why the combination of pharmacological properties is unique among currently available antiepileptic drugs and may explain why TPM is effective in both partial and generalized seizures [36].

3.5. NMR spectra in both media.

Here, the theoretical ^{1}H- and ^{13}C-NMR spectra were predicted for topiramate in aqueous solution by using the B3LYP/6-311++G** level of theory and the GIAO method [31]. Then, the predicted ^{1}H- and ^{13}C-NMR chemical shifts were compared with the experimental available for topiramate in DMSO-*d6* taken from Ref [7] by using the root-mean-square deviation (RMSD) values. In Tables S6 and S7 have presented the comparisons of predicted ^{1}H- and ^{13}C-NMR chemical shifts by using RMSD values. Very good correlations with low RMSD values were obtained for the TPM gas phase and aqueous solution with values between 0.42 and 0.38 ppm for the H atoms, while for the C atoms, the RMSD values increase to 4.69 and 5.01 ppm. These low RMSD values for topiramate suggest that the two structures in both media can be used to perform the vibrational studies and the determinations of corresponding harmonic force fields.

3.6. Vibrational study.

In the published tentative vibrational assignments of topiramate by Sena *et al*. [4], with the B3LYP/6-31G* method using the Gaussian 98 package, some vibration modes corresponding to the SO_3 group considered with C_{3v} symmetry have not been descript correctly because they have assigned three symmetric and only one antisymmetric SO_3 modes instead of two antisymmetric and one symmetric SO_3 modes. Moreover, they have reported only the antisymmetric and symmetric stretching modes for the NH_2 group while the deformation, wagging, rocking, and twisting modes expected for this group were not assigned. In this study, we have performed the complete assignments of 123 vibration modes of TPM in the gas phase with the B3LYP/6-311++G** level of theory and taking into account two harmonic force fields. Hence, the normal internal coordinates of the sulfamate group (O-SO_2-NH_2) of TPM have been defined of two forms: in one case, both SO_2 and NH_2 groups were considered with C_{2V} symmetries, and, in the other one, the NH_2 and SO_3 groups present C_{2V} and C_{3V} symmetries, respectively. On the other hand, each pair of methyl groups was considered with C_{2V} symmetry. The B3LYP/6-311++G** level of theory has optimized the TPM structures in both media with C_1 symmetries and its expected 123 vibration modes present activity in the infrared and Raman spectra. The predicted infrared and Raman spectra of TPM in both media are compared in Figures 5 and 6 with the corresponding available taken from Ref [22] for TPM in the solid-state. Reasonable correlations were found between the predicted spectra with the corresponding available ones, as can be seen in Figs 5 and 6. The predicted Raman spectrum in activities was corrected to intensities with known equations [23,24]. Note that the intensities of some bands change in the predicted spectra in solution and, in particular, in the Raman spectrum, as shown in Figure 6.

In the determination of the two harmonic force fields of TPM were used the two definitions of normal internal coordinates of sulfamate group (O-SO_2-NH_2) and the scaled quantum mechanical force field (SQMFF) methodology with the Molvib program [11-13].

Transferable scaling factors and potential energy distribution (PED) contributions ≥ 10% were employed to perform the vibrational assignments.

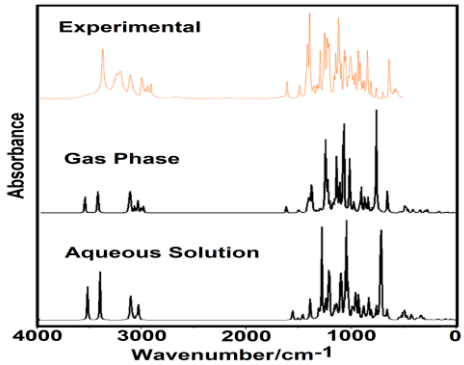

Figure 5. Experimental available Infrared spectra of TPM in solid phase [22] compared with the predicted in the gas phase and solution by using the hybrid B3LYP/6-311++G** method.

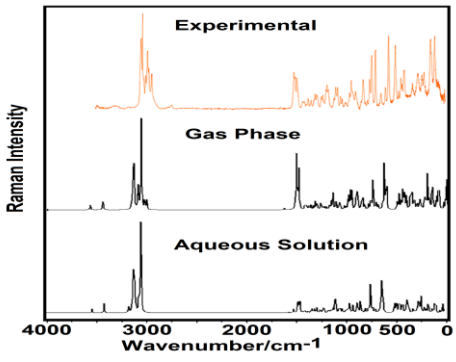

Figure 6. Experimental available Raman spectra of TPM in solid phase [22] compared with the predicted in the gas phase and solution by using the hybrid B3LYP/6-311++G** method.

Observed and calculated wavenumbers for TPM in the gas phase by using B3LYP/6-311++G** calculations and the corresponding assignments for the two proposed harmonic force fields can be seen in Table 5. The two calculated harmonic force fields for TPM can be obtained upon request. Then, some important assignments taking into account the two proposed force fields are discussed below.

Table 5. Observed and calculated wavenumbers (cm^{-1}) together with two assignments proposed for Topimarate in the gas phase by using the B3LYP/6-311++G** method.

Experimental			**B3LYP/6-311++G** method[a]**					
			Calc.[b]	Int.[c]	NH_2 (C_{2v}), SO_2 (C_{2v})		NH_2 (C_{2v}), SO_3 (C_{3v})	
ATR	IR	Raman			SQM[d]	Assignments[a]	SQM[d]	Assignments[a]
3396sh	3444sh	3395w	3578	74.7	3430	ν_aNH_2	3430	ν_aNH_2
3381w	3376s		3452	132.5	3310	ν_sNH_2	3310	ν_sNH_2
3241sh	3237m	3236w	3165	12.9	3034	ν_aCH_3(C19)	3034	ν_aCH_3(C19)
3212w	3208m		3156	2.0	3025	ν_aCH_2(C18)	3025	ν_aCH_2(C18)
3112w	3111m	3120w	3152	27.1	3022	ν_aCH_3(C22)	3022	ν_aCH_3(C22)
			3148	23.4	3018	ν_aCH_3(C20)	3018	ν_aCH_3(C20)
			3148	23.7	3017	ν_aCH_3(C22)	3017	ν_aCH_3(C22)
			3146	19.3	3016	ν_aCH_3(C20)	3016	ν_aCH_3(C20)
			3143	22.4	3013	ν_aCH_3(C21)	3013	ν_aCH_3(C21)
			3139	7.8	3009	ν_aCH_2(C15)	3009	ν_aCH_2(C15)
			3139	20.5	3009	ν_aCH_3(C21)	3009	ν_aCH_3(C21)
3008sh		3009vs	3138	3.0	3008	ν_aCH_3(C19)	3008	ν_aCH_3(C19)
2999w	2997m	2996vs	3102	11.9	2974	ν_sCH_2(C18)	2974	ν_sCH_2(C18)
2987sh		2968m	3101	22.9	2973	νC14-H25	2973	νC14-H25
2960w	2957w	2952s	3073	16.6	2946	ν_sCH_3(C22)	2946	ν_sCH_3(C22)
2960w	2957w	2952s	3072	12.6	2945	ν_sCH_3(C19)	2945	ν_sCH_3(C19)
			3071	10.5	2944	ν_sCH_2(C15)	2944	ν_sCH_2(C15)
2940w	2936w	2938s	3067	7.2	2940	ν_sCH_3(C20)	2940	ν_sCH_3(C20)
			3065	12.2	2939	ν_sCH_3(C21)	2939	ν_sCH_3(C21)
2911w	2903m	2916m	3037	26.2	2911	νC12-H24	2911	νC12-H24
			3016	25.1	2892	νC11-H23	2892	νC11-H23
1571w	1574m		1646	29.3	1573	δNH_2	1573	δNH_2
	1467sh	1461s	1538	5.1	1470	δCH_2(C15)	1470	δCH_2(C15)
			1528	4.9	1460	δ_aCH_3(C19)	1460	δ_aCH_3(C19)
	1460sh		1527	5.6	1459	δ_aCH_3(C22)	1459	δ_aCH_3(C22)
	1460sh		1526	0.8	1459	δ_aCH_3(C22)	1459	δ_aCH_3(C22)

Experimental			B3LYP/6-311++G** method[a]					
			Calc.[b]	Int.[c]	NH_2 (C_{2v}), SO_2 (C_{2v})		NH_2 (C_{2v}), SO_3 (C_{3v})	
ATR	IR	Raman			SQM[d]	Assignments[a]	SQM[d]	Assignments[a]
			1525	0.8	1458	$\delta_a CH_3$(C20)	1458	$\delta_a CH_3$(C20)
1446w	1452m	1451s	1509	0.7	1442	$\delta_a CH_3$(C21)	1442	$\delta_a CH_3$(C21)
	1445sh		1509	1.3	1442	$\delta_a CH_3$(C19)	1442	$\delta_a CH_3$(C19)
			1508	4.3	1441	δCH_2(C18)	1441	δCH_2(C18)
	1438sh	1436s	1504	0.1	1437	$\delta_a CH_3$(C21)	1437	$\delta_a CH_3$(C21)
	1438sh		1503	0.0	1437	$\delta_a CH_3$(C20)	1437	$\delta_a CH_3$(C20)
			1445	24.2	1399	ρC12-H24	1399	ρC12-H24
1383sh	1384sh	1386w	1444	17.6	1381	$\delta_s CH_3$(C20)	1381	$\delta_s CH_3$(C20)
			1440	4.9	1380	$\delta_s CH_3$(C22)	1380	$\delta_s CH_3$(C22)
1370m	1374s	1370w	1432	23.8	1376	ρ'C14-H25,$\delta_s CH_3$(C20)	1376	ρ'C14-H25, $\delta_s CH_3$(C20)
			1430	21.9	1372	$\delta_s CH_3$(C21)	1372	$\delta_s CH_3$(C21)
1367sh			1422	35.7	1367	$\delta_s CH_3$(C19)	1367	$\delta_s CH_3$(C19)
			1412	19.0	1364	wagCH_2(C18)	1364	wagCH_2(C18)
			1403	174.9	1362	ρC11-H23	1362	ρC11-H23
1348s	1356vs	1354w	1402	0.5	1352	$\nu_a SO_2$	1351	$\nu_a SO_3$
		1338w	1384	3.9	1334	ρCH_2(C15) ρC14-H25	1334	ρCH_2(C15)
			1359	9.6	1326	ρ'C11-H23	1326	ρ'C11-H23
1317w	1313w	1310w	1343	5.6	1310	ρ'C12-H24	1310	ρ'C12-H24
1309w	1288w	1288w	1325	18.7	1298	ρCH_2(C18),νC11-C12	1298	ρCH_2(C18), νC11-C12
1284w	1288w	1278m	1317	10.9	1281	ρ'C14-H25	1281	ρ'C14-H25,ρC14-H25
1276w	1277w	1266m	1290	17.0	1255	wagCH_2(C15)	1255	wagCH_2(C15)
1245s	1248s	1250sh	1280	9.8	1240	νC17-C22, ρCH_3(C21)	1240	νC17-C22, ρCH_3(C21)
		1234sh	1270	270.8	1230	βR_1(A2),ρCH_3(C20)	1230	βR_1(A2),ρCH_3(C20)
1219sh	1223sh	1223m	1265	46.8	1223	νC16-C20,νC16-C19	1223	νC16-C20,νC16-C19
1201s	1209s	1208m	1250	141.0	1208	νC17-C21	1208	νC17-C21
1177s	1184s	1182m	1231	32.5	1186	wagCC_2(C16)	1186	νC13-O4
1168s	1177s	1173s	1204	20.5	1165	ρNH_2	1165	ρNH_2
1168s	1163s		1197	30.4	1162	wagCC_2(C17)ρCH_3(C22)	1162	wagCC_2(C17) ρCH_3(C22)
1159s		1159m	1184	32.4	1156	νC13-C18	1156	νC13-C18
1159s		1159m	1167	159.5	1126	$\nu_s SO_2$νC13-C11	1126	νC13-C11
1159s			1162	109.5	1119	$\nu_s SO_2$	1119	$\nu_s SO_3\nu_a SO_3$
1107	1112sh	1111m	1138	14.2	1101	νC14-C15,νC13-C11	1101	νC14-C15
1094s	1101s	1097s	1137	92.1	1088	νC11-O2	1088	νC11-O2
1063vs	1069vs	1081s	1115	8.9	1065	νC12-O5	1065	νC14-O6
	1062sh	1057m	1104	125.3	1059	νC15-O3,νC14-O6	1059	νC15-O3,νC14-O6
1054s			1097	311.6	1055	νC15-O3	1055	νC15-O3
1039s	1044s	1041w	1093	29.3	1043	νC14-O6	1043	νC14-O6,νC15-O3
	1016s	1016w	1058	6.4	1013	νC15-O3,νC14-C15	1013	νC15-O3,νC14-C15
1006s	1005s	1007w	1042	232.9	1001	νC18-O7	1001	νC18-O7
997s	994sh	986sh	1018	0.1	976	ρ'CH_3(C20),ρ'CH_3(C19)	976	ρ'CH_3(C20),ρ'CH_3(C19)
971m	972m	976m	1018	0.5	975	ρ'CH_3(C21),ρCH_3(C22)	975	ρ'CH_3(C21) ρCH_3(C22)
	958sh	962s	1010	6.4	962	τwCH_2(C15)	962	νC12-O5,τwCH_2(C15)
954sh	951s	952m	1000	37.8	958	ρCH_3(C20)ρCH_3(C19)	958	ρCH_3(C20)
945s			985	8.8	945	ρCH_3(C21),ρ'CH_3(C22)	945	ρCH_3(C21) ρ'CH_3(C22)
920w	922w	926m	947	38.7	902	ρCH_3(C19) ρCH_3(C20)	902	ρCH_3(C19)
901m	908m	896sh	939	8.5	896	ρCH_3(C21),ρ'CH_3(C22)	896	ρCH_3(C21) ρ'CH_3(C22)
872vs	876s	874w	936	0.4	892	νC13-O4,τwCH_2(C18)	892	τwCH_2(C18)
853s	858s	858s	928	88.9	887	wagNH_2	887	wagNH_2
847sh			893	75.6	862	νC16-O2	862	νC16-O2
831m	837w	842w	883	8.4	847	νC17-O5	847	νC17-O5
816m	822w	822w	862	70.6	827	νC16-O2,νC17-O5	827	νC16-O2,νC17-O5
796sh	786s	801s	824	15.3	794	νC16-O4	794	νC16-O4
780vs		783vs	804	18.1	776	νC17-O6,βR_1(A3)	776	νC17-O6,βR_1(A3)
780vs			785	345.5	757	νC13-O3	757	νC13-O3

Experimental			B3LYP/6-311++G** method[a]					
			Calc.[b]	Int.[c]	NH_2 (C_{2v}), SO_2 (C_{2v})		NH_2 (C_{2v}), SO_3 (C_{3v})	
ATR	IR	Raman			SQM[d]	Assignments[a]	SQM[d]	Assignments[a]
747s	750m	750vs	782	84.4	754	νN10-S1	754	νN10-S1
730sh		733vw	754	7.1	727	νC12-C14,βR_1(A1)	727	βR_1(A1)
695s	700w	703m	735	5.2	714	βR_2(A3)	714	βR_2(A3)
660w	668vw	664m	697	2.2	674	βR_2(A2)	674	βR_2(A2)
629m	639w	636vs	679	81.1	654	νO7-S1	654	$\delta_{as}SO_3$,ν_sSO_3
629m	639w	636vs	661	0.1	647	νC17-C22	647	νC17-C22
568vs	575s	576vs	658	7.3	638	βR_1(A2)	638	βR_1(A2)
546w	557sh	548m	562	6.8	548	τwCC_2(C16)	548	τwCC_2(C16)
524m	528w	528s	545	5.8	528	δC18O7S1,τ_wSO_2	528	δC18O7S1, δ_sSO_3
513s	521w	518m	527	4.8	515	ρSO_2	515	$\delta_{as}SO_3$
498m	503w	500s	512	12.5	502	τwCC_2(C17)	502	τwCC_2(C17)
498m	503w	500s	509	15.9	500	τwCC_2(C16)	500	δ_sSO_3
490m			498	26.1	491	τwCC_2(C17), τwCC_2(C16)	491	$\delta_{as}SO_3$, δ_sSO_3
452sh	467w	455w	480	12.0	469	δSO_2	469	$\delta_{as}SO_3$
434sh		427m	444	6.1	429	wagCC_2(C17)ρ'C18-C13	429	wagCC_2(C17)ρ'C18-C13
422m			433	13.7	417	wagSO_2	417	ρ'SO_3
408m			418	2.6	405	ButC11-C13	405	ButC11-C13
395w		393sh	410	0.7	401	τR_1(A1),βR_3(A1)	401	βR_3(A1),βR_2(A1)
		377s	387	2.9	379	wagCC_2(C16)	378	wagCC_2(C16)
			369	10.6	359	ButC12-C14	359	ButC12-C14
		349sh	360	7.3	352	δO7S1N10	352	ρSO_3
		341s	347	1.0	341	δCC_2(C17), ρCC_2(C17) τR_1(A1)	341	δCC_2(C17), ρCC_2(C17) τR_1(A1)
		326s	326	2.0	319	δCC_2(C16)	319	δCC_2(C16)
		319sh	319	8.7	309	ρCC_2(C16), τR_3(A1)	309	ρCC_2(C16),τR_3(A1)
			311	3.2	303	ρCC_2(C16)	303	ρCC_2(C16)
		281sh	296	13.5	280	τwNH_2	280	τwNH_2
		269vs	278	1.2	264	wagSO_2,τwNH_2	264	$\delta_{as}SO_3$
		234vs	255	0.3	239	δO7S1N10	239	$\delta_{as}SO_3$
			253	0.3	229	τ_wCH_3(C21)	229	τ_wCH_3(C21)
		226sh	246	1.1	228	τ_wCH_3(C19)	228	τ_wCH_3(C19)
		212sh	215	0.1	200	τ_wCH_3(C21)	200	τ_wCH_3(C21)
		200sh	209	0.4	193	τ_wCH_3(C20)	193	τ_wCH_3(C20)
		190sh	196	0.1	184	δC18O7S1	184	δC18O7S1
			190	0.6	177	τ_wCH_3(C22)	177	τ_wCH_3(C22)
		164sh	180	11.6	173	δO7C18C13,τO7-S1	173	δO7C18C13
			131	4.2	123	τO7-S1,ρC18-C13	123	τ_wSO_3,ρC18-C13
			109	0.6	106	τR_1(A3),τR_3(A1)	106	τR_1(A3), τR_3(A1)
			94	3.8	89	τR_1(A2), τR_2(A1)	89	τR_1(A2),τR_2(A1)
			90	0.8	86	τR_2(A1)	86	τR_2(A1)
			56	2.3	53	τR_2(A3)	53	τR_2(A3)
			49	1.2	48	τR_1(A2), τR_2(A2)	48	τR_1(A2), τR_2(A2)
			42	1.2	39	τC18-O7	39	τC18-O7
			29	1.3	26	τ_wC18-C13	26	τ_wC18-C13

Abbreviations: ν, stretching; β, deformation in the plane; γ, deformation out of the plane; τ, torsion; β_R. deformation ring τ_R, torsion ring; ρ, rocking; τw, twisting; δ, deformation; a, antisymmetric; s, symmetric; (A_1), Ring R1; (A_2), Ring R2; (A_3), Ring R3; [a]This work, [b]Intensities in KM/Mole; [c]From B3LYP/6-311++G** method, [d]From scaled quantum mechanics force field.

3.6.1. Case 1. C_{2v} symmetries for both SO_2 and NH_2 groups.

3.6.1.1. 4000-2000 cm^{-1} region.

In this region, for TPM are expected the antisymmetric and symmetric stretching modes corresponding to NH_2, three CH_3, and two CH_2 groups and also to the aliphatic stretching

modes of three C-H groups. The two stretching modes of the NH_2 group are predicted at 3430 and 3310 cm^{-1}; hence, the shoulders and IR and Raman bands located between 3444 and 3376 cm^{-1} are assigned to these vibration modes. The assignments for the other two groups are perfectly detailed in Table 5. Note that the C14-H25 stretching mode is predicted to higher wavenumbers than the other ones, probably because it is next to the O6 atom belonging to the R2 ring. These assignments are in agreement with reported for compounds containing similar groups [18-21,33-35,37].

3.6.1.2. 2000-1000 cm^{-1} region.

In this region are expected the antisymmetric and symmetric stretching modes of SO_2 groups, the C-C and C-O stretching modes, and the deformation, wagging, and rocking modes of CH_3 and CH_2 groups in addition to the deformation and rocking modes of NH_2 and aliphatic C-H groups. Thus, the IR and Raman bands at 1571 and 1574 cm^{-1} are assigned to NH_2 deformation mode while the strong IR and Raman bands respectively at 1168 and 1177 cm^{-1} are assigned to corresponding rocking mode. The strong IR bands at 1348 and 1159 cm^{-1} are assigned to SO_2 antisymmetric and symmetric modes as predicted by calculations and according to similar compounds [18-21]. The C-C stretching modes are predicted from 1240 to 647 cm^{-1} while the C-O stretching modes from 1088 to 757 cm^{-1}. Hence, the experimental bands observed in both spectra between 1240 and 647 cm^{-1} can be assigned to these vibration modes, as predicted by SQM calculations and as reported in the literature [33-35,37].

3.6.1.3. 1000-20 cm^{-1} region.

In Table 5 can be observed the expected vibration modes of TPM in this region. Thus, the deformation, wagging, rocking, and twisting modes of SO_2 and wagging and twisting modes of the NH_2 group are predicted in this region. On the other hand, the N10-S1 and O7-S1 stretching modes corresponding to the sulfamate group of TPM are also expected in this region. Here, the IR and Raman bands at 467, 422, 513, and 524 cm^{-1} are assigned respectively to deformation, wagging, rocking, and twisting modes of the SO_2 group while the bands at 853 and 281 cm^{-1} are assigned to wagging and twisting modes of NH_2 group. The SQM calculations predict the wagging SO_2 mode coupled with the twisting NH_2 mode at 264 cm^{-1}, for which the very strong Raman band at 269 cm^{-1} can also be assigned to those two vibration modes. The strong and medium intensity bands at 747 and 629 cm^{-1} can be assigned respectively to the N10-S1 and O7-S1 stretching modes, as predicted by the SQM calculations. The vibration modes of six and five-membered rings are assigned according to the theoretical calculations and be reported for compounds with similar rings [18-21,33-35,37].

3.6.2. Case 2. C_{3V} and C_{2V} symmetries for both SO_3 and NH_2 groups.

3.6.2.1. 4000-2000 cm^{-1} region.

In this region, the vibrational assignments for TPM are exactly similar for those proposed for case 1, as observed in Table 5.

3.6.2.2. 2000-1000 cm^{-1} region.

In this region and from 2000 to 1200 cm^{-1}, the assignments for case 2 are the same that for case 1 and, from 1186 to 1039 $cm^{-1,}$ some assignments have changed. Thus, the strong IR

band at 1177 cm^{-1} is assigned to C13-O4 stretching mode, while the strong IR band at 1159 cm^{-1} can be simultaneously assigned to C13-C11 and C14-C15 stretching modes and to antisymmetric and symmetric stretching modes of the SO_3 group. Then, the strong IR band at 1039 cm^{-1} is assigned to the C14-O6 and C15-O3 stretching modes.

3.6.2.3. 1000-20 cm^{-1} region.

In this region are observed the higher variations in the assignments de some groups for case 2. Hence, some rocking modes of CH_3 groups and twisting mode of CH_2 (C18) are predicted by calculations as pure modes, without coupling, while other vibration modes from 654 up to 349 cm^{-1} and from 264 to 239 cm^{-1} change completely with the case 2 is considered, as detailed in Table 5. The expected assignments of deformations and torsions of six and five members' rings were performed according to the SQM calculations and to assignments reported for compounds with similar rings [18-21,33-35,37,38].

The two proposed assignments for TPM considering both harmonic force fields are well represented because the calculated harmonic vibrational frequencies are consistent with the experimental IR and Raman spectra in the solid phase.

Table 6. Scaled internal force constants for topiramate in gas phase and aqueous solution by using the B3LYP/6-311++G** method.

Force constant	**B3LYP/6-311++G** method[a]**			
	Camphor			
	NH_2 (C_{2V}), SO_2 (C_{2V})		NH_2 (C_{2V}), SO_3 (C_{3V})	
	Gas	PCM	Gas	PCM
f(νC-H)	4.71	4.71	4.71	4.71
f(νC-O)	4.46	4.46	4.46	4.46
f(νS=O)	9.26	9.26	7.32	7.32
f(νS-O)	3.43	3.43		
f(νNH_2)	6.31	6.31	6.31	6.31
f(νCH_2)	4.92	4.92	4.92	4.92
f(νCH_3)	4.94	4.94	4.94	4.94
f(δNH_2)	0.63	0.63	0.63	0.63
f(δSO_2)	1.80	1.80	1.76	1.76
f(δCH_2)	0.78	0.78	0.78	0.78
f(δCH_3)	0.54	0.54	0.54	0.54

Units are mdyn $Å^{-1}$ for stretching and mdyn Å rad^{-2} for angle deformations; [a]This work

3.7. Force fields.

The scaled force constants of TPM in both media were determined for the two proposed harmonic force fields by using the B3LYP/6-311++G** method, the SQMFF methodology, and the Molvib program [11-13]. These force constants are shown in Table 6.

When the values for each case are compared in both media, it is observed that all force constants do not change; however, when the force constants for the case 1 are compared with the corresponding to case 2 we observed that only the *f(νS=O)* and *f(δSO_2)* force constants values have changed, as expected. Such observation is justified because, in case 1, the sulfamate group was considered as an SO_2 group where the two involved S=O bonds have double bonds characteristics, while in case 2, that SO_3 group has three S-O bonds with characteristics of simple bonds.

Hence, lower values are expected for those two force constants in case 2. On the other hand, the *f(νSO₃)* and *f(δSO₃)* force constants values observed for the SO_3 group of TPM are in agreement with those observed for the sulfonate group of 1-Butyl-3-methylimidazolium trifluoromethanesulfonate ionic liquid, with values of 7.63 mdyn $Å^{-1}$ and 1.62 mdyn Å rad^{-2}, respectively [18]. Whereas the *f(νS=O)* and *f(δSO₂)* force constants values of TPM are in agreement with the reported for the neutral form of cyclamic acid (9.02 mdyn $Å^{-1}$ and 1.87 mdyn Å rad^{-2}) [19]. The *f(νNH₂)* and *f(δNH₂)* force constants obtained for TPM with both force fields present approximately similar values to the reported for the antiviral cidofovir agent (6.79 mdyn $Å^{-1}$ and 0.70 mdyn Å rad^{-2}) [33]. Finally, the *f(νCH₃)* and *f(νCH₂)* force constants for both TPM cases show good concordances with the reported for the free base of promethazine (4.82 and 4.74 mdyn $Å^{-1}$) [37].

3.8. Ultraviolet-visible spectra.

The electronic spectra of TPM in aqueous solution was predicted by using the B3LYP/6-311++G** method and TD-DFT calculations with the Gaussian 09 program [10]. The same presents an intense band in c.a. 185 nm and can be seen in Figure 7 [39]. Experimentally TPM cannot be analyzed by ultraviolet spectroscopic methods, as mentioned by Khalil *et al*. because it species does not contain any chromospheres that could yield absorbance bands above 190 nm [7]. That strong band predicted by using the B3LYP/6-311++G** method could be associated with $n \rightarrow \sigma^*$ interactions, as supported by NBO calculations.

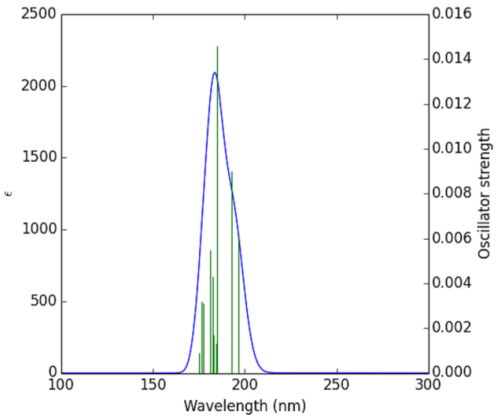

Figure 7. Predicted Ultraviolet-visible spectra of topiramate in aqueous solution by using the B3LYP/6-311++G** method.

4. Conclusions

The theoretical structures of topiramate in the gas phase and aqueous solution have been determined by using the hybrid B3LYP/6-311++G** method. Very good concordances were found between the theoretical structures and the corresponding experimental reported. Thus, the fused five-membered ring in topiramate produces that the pyranose ring adopts distorted twist-boat conformation, as was experimentally observed. The calculated N10-O3 distance between the N atom and the O3 pyranose ring oxygen atom (3.349 and 3.867 Å), different from the experimental value (5.965 Å), could justify the biological activity of TPM because the N10-O3 distance connects the hydrophilic part with the corresponding hydrophobic one. In solution, all calculations were performed with the SCRF method and the IEFPCM and SMD models.

The corrected solvation energy value for topiramate in aqueous solution by total non-electrostatic terms and by ZPVE is -1066.10 kJ/mol.

The bond orders have evidenced that the three O atoms are not linked to the same form to S atom. Hence, the S atom of TPM is practically tetra-coordinate in both media, as evidenced by the high negative MK and NPA charges on the O atoms linked to it.

The AIM study supports the higher stability of TPM in the gas phase while the NBO study suggests the higher stability in solution.

The studies by using the frontier orbitals suggest that TPM is slightly most reactive in solution.

The complete assignments of 123 vibration modes of TPM are reported with the B3LYP/6-311++G** level of theory and taking into account two harmonic force fields. In one case, the normal internal coordinates of both SO_2 and NH_2 groups have been considered with C_{2V} symmetries, and, in the other one, the NH_2 and SO_3 groups present C_{2V} and C_{3V} symmetries, respectively. The scaled force constant for both cases is reported for the first time.

Comparisons of predicted ^{1}H- and ^{13}C-NMR spectra with the corresponding experimental ones reveal very good concordances.

Funding

This research received no external funding.

Acknowledgments

This work was supported with grants from CIUNT Project Nº 26/D608 (Consejo de Investigaciones, Universidad Nacional de Tucumán).

Conflicts of Interest

The authors declare no conflict of interest.

Supporting Information Available

Tables from S1-S2 and Figures S1-S7.

References

1. Kubicki, M.; Codding, P.W.; Litster, S.A.; Szkaradziñska, M.B.; Bassyouni, H.A.R. Pyranose sulfamates: conformation and hydrogen bonding. *J. Mol. Struct.* **1999**, *474*, 255-265, https://doi.org/10.1016/S0022-2860(98)00578-X.
2. Abbate, F.; Winum, J-Y; Potter, B.V.L.; Casini, A.; Montero, J-L; Scozzafava, A.; Supuran, C.T. Carbonic anhydrase inhibitors: X-ray crystallographic structure of the adduct of human isozyme II with EMATE, a dual inhibitor of carbonic anhydrases and steroid sulfatase. *Bioorganic & Medicinal Chemistry Letters* **2004**, *14*, 231–234, https://doi.org/10.1016/j.bmcl.2003.11.014.
3. Abbate, F.; Coetzee, A.; Casini, A.; Ciattini, S.; Scozzafavac, A.; Supuran, C.T. Carbonic anhydrase inhibitors: X-ray crystallographic structure of the adduct of human isozyme II with the antipsychotic drug sulpiride. *Bioorganic & Medicinal Chemistry Letters* **2004**, *14*, 337–341, https://doi.org/10.1016/j.bmcl.2003.09.064.
4. Sena Jr., D.M.; Freire, P.T.C.; Filho, J.M.; Melo, F.E.A.; Pontes, F.M.; Longo, E.; Ferreirae, O.P.; Alves, O.L. Vibrational and Thermal Properties of Crystalline Topiramate. *J. Braz. Chem. Soc*. **2008**, *19*, 1607-1613, https://doi.org/10.1590/S0103-50532008000800022.
5. Ghiasi, M.; Oskouie, A.A.; Saeidian, H. Dynamic stereochemistry of topiramate (anticonvulsant drug) in solution: theoretical approaches and experimental validation. *Carbohydrate Research* **201**2, *348*, 47–54, https://doi.org/10.1016/j.carres.2011.11.010.

6. Ghiasi, M.; Kamalinahad, S. Conformational Analysis of Topiramate and Related Anion in the Solution and Interaction Between the Most Stable Conformer of Topiramate with Active Center of Carbonic Anhydrase Enzyme. *Journal of Carbohydrate Chemistry* **2015**, *34*, 80–102, http://dx.doi.org/10.1080/07328303.2015.1009090.
7. Khalil, N.Y.; AlRabiah, H.K.; AL Rashoud, S.S.; Bari, A.; Wani, T.A. Topiramate, Comprehensive profile, Profiles of Drug Substances, Excipients, and Related Methodology. *Elsevier Inc.* **2019**, *44*, https://doi.org/10.1016/bs.podrm.2018.11.005.
8. Becke, A.D. Density-functional exchange-energy approximation with correct asymptotic behavior. *Phys. Rev*. **1988**, *A38*, 3098-3100, https://doi.org/10.1103/PhysRevA.38.3098.
9. Lee, C.; Yang, W.; Parr, R.G. Development of the Colle-Salvetti correlation-energy formula into a functional of the electron density. *Phys. Rev*. **1988**, *B37*, 785-789, https://doi.org/10.1103/PhysRevB.37.785.
10. Frisch, M.J.; Trucks, G.W.; Schlegel, H.B.; Scuseria, G.E.; Robb, M.A.; Cheeseman, J.R.; Scalmani, G.; Barone, V.; Mennucci, B.; Petersson, G.A.; Nakatsuji, H.; Caricato, M.; Li, X.; Hratchian, H.P.; Izmaylov, A.F.; Bloino, J.; Zheng, G.; Sonnenberg, J.L.; Hada, M.; Ehara, M.; Toyota, K.; Fukuda, R.; Hasegawa, J.; Ishida, M.; Nakajima, T.; Honda, Y.; Kitao, O.; Nakai, H.; Vreven, T.; Montgomery, J.A.; Peralta, J.E.; Ogliaro, F.; Bearpark, M.; Heyd, J.J.; Brothers, E.; Kudin, K.N.; Staroverov, V.N.; Kobayashi, R.; Normand, J.; Raghavachari, K.; Rendell, A.; Burant, J.C.; Iyengar, S.S.; Tomasi, J.; Cossi, M.; Rega, N.; Millam, J.M.; Klene, M.; Knox, J.E.; Cross, J.B.; Bakken, V.; Adamo, C.; Jaramillo, J.; Gomperts, R.; Stratmann, R.E.; Yazyev, O.; Austin, A.J.; Cammi, R.; Pomelli, C.; Ochterski, J.W.; Martin, R.L.; Morokuma, K.; Zakrzewski, V.G.; Voth, G.A.; Salvador, P.; Dannenberg, J.J.; Dapprich, S.; Daniels, A.D.; Farkas, O.; Foresman, J.B.; Ortiz, J.; Cioslowski, J.; Fox, D.J. Gaussian, Inc., Wallingford CT, **2009**.
11. Pulay, P.; Fogarasi, G.; Pongor, G.; Boggs, J.E.; Vargha, A. Combination of theoretical ab initio and experimental information to obtain reliable harmonic force constants. Scaled quantum mechanical (QM) force fields for glyoxal, acrolein, butadiene, formaldehyde, and ethylene. *J. Am. Chem. Soc*. **1983**, *105*, 7037-7047, https://doi.org/10.1021/ja00362a005.
12. Rauhut, G.; Pulay, P. Transferable Scaling Factors for Density Functional Derived Vibrational Force Fields. *J. Phys. Chem*. **1995**, *99*, 3093-3100, https://doi.org/10.1021/j100010a019
13. Sundius, T. Scaling of ab-initio force fields by MOLVIB. *Vib. Spectrosc*. **2002**, *29*, 89-95, https://doi.org/10.1016/S0924-2031(01)00189-8.
14. Miertus, S.; Scrocco, E.; Tomasi, J. Electrostatic interaction of a solute with a continuum. *Chem. Phys.* **1981**, *55*, 117–129, https://doi.org/10.1016/0301-0104(81)85090-2.
15. Tomasi, J.; Persico, J. Molecular Interactions in Solution: An Overview of Methods Based on Continous Distributions of the Solvent. *Chem. Rev*. **1994**, *94*, 2027-2094, https://doi.org/10.1021/cr00031a013.
16. Marenich, A.V.; Cramer, C.J.; Truhlar, D.G. Universal solvation model based on solute electron density and a continuum model of the solvent defined by the bulk dielectric constant and atomic surface tensions. *J. Phys. Chem.* **2009**, *B113*, 6378-6396, https://doi.org/10.1021/jp810292n.
17. Paar, R.G.; Pearson, R.G. Absolute hardness: companion parameter to absolute electronegativity. *J. Am. Chem. Soc.* **1983**, *105*, 7512-7516, https://doi.org/10.1021/ja00364a005.
18. Kausteklis, J.; Aleksa, V.; Iramain, M.A.; Brandán, S.A. DFT study and vibrational assignment of 1-Butyl-3-methylimidazolium trifluoromethanesulfonate ionic liquid by using the FT-Raman spectrum. *J Mol. Struct.* **2019**, *1175*, 663-676. https://doi.org/10.1016/j.molstruc.2018.08.014.
19. Brizuela, A.B.; Raschi, A.B.; Castillo, M.V.; Davies, L.; Romano, E.; Brandán, S.A. Structural and vibrational investigation on species derived from cyclamic acid in aqueous solution by using HATR and Raman spectroscopies and SCRF calculations. *J. Mol. Struct*. **2014**, *1074*, 144-156, http://dx.doi.org/10.1016/j.molstruc.2014.05.019.
20. Ben M'leh, C.; Brandán, S.A.; Issaoui, N.; Roisnel, T.; Marouani, H. Synthesis, molecular structure, vibrational and theoretical studies of a new non-centrosymmetric organic sulphate with promising NLO properties. *J Mol. Struct.* **2018**, *1171*, 771-785, https://doi.org/10.1016/j.molstruc.2018.06.041.
21. Noureddine, O.; Gatfaoui, S.; Brandán, S.A.; Marouani, H.; Issaoui, N. Structural, docking and spectroscopic studies of a new piperazine derivative, 1-Phenylpiperazine-1,4-diium-bis (hydrogen sulfate). *J Mol. Struct*. **2020**, *1202*, https://doi.org/10.1016/j.molstruc.2019.127351.
22. Experimental available ATR, IR and Raman spectra of topiramate from: https://spectrabase.com/spectrum/
23. Keresztury, G.; Holly, S.; Besenyei, G.; Varga, J.; Wang, A.Y.; Durig, J.R. Vibrational spectra of monothiocarbamates-II. IR and Raman spectra, vibrational assignment, conformational analysis and *ab initio* calculations of *S*-methyl-*N*,*N*-dimethylthiocarbamate. *Spectrochim. Acta* **1993**, *49A*, 2007-2026, https://doi.org/10.1016/S0584-8539(09)91012-1.
24. Michalska, D.; Wysokinski, R. The prediction of Raman spectra of platinum(II) anticancer drugs by density functional theory. *Chemical Physics Letters* **2005**, *403*, 211-217, https://doi.org/10.1016/j.cplett.2004.12.096.
25. Glendening, E.; Badenhoop, J.K.; Reed, A.D.; Carpenter, J.E.; Weinhold, F. NBO 3.1. Theoretical Chemistry Institute, University of Wisconsin; Madison, WI, **1996**.
26. Bader, R.F.W. *Atoms in Molecules, A Quantum Theory.* Oxford University Press, Oxford, **1990.**

27. Biegler-Köning, F.; Schönbohm, J.; Bayles, D. AIM2000; A Program to Analyze and Visualize Atoms in Molecules. *J. Comput. Chem.* **2001**, *22*, http://dx.doi.org/10.1002/1096-987X(20010415)22:5%3C545::AID-JCC1027%3E3.0.CO;2-Y
28. Besler, B.H.; Merz, J.K.M.; Kollman, P.A. Atomic charges derived from semiempirical methods. *J. Comp. Chem.* **1990**, *11*, 431-439, https://doi.org/10.1002/jcc.540110404.
29. Nielsen, A.B.; Holder, A.J. *Gauss View 3.0. User's Reference*. Gaussian Inc., Pittsburgh, PA, **2000–2003**.
30. Ugliengo, P. Moldraw Program, University of Torino, Dipartimento Chimica IFM, Torino, Italy, **1998**.
31. Ditchfield, R. Self-consistent perturbation theory of diamagnetism. I. A gage-invariant LCAO (linear combination of atomic orbitals) method for NMR chemical shifts. *Mol Phys*. **1974**, *27*, 714–722.
32. Iramain, M.A.; Brandán, S.A. Structural and vibrational study on the acid, hexa-hydrated and anhydrous trisodic salts of antiviral drug Foscarnet. *Drug Designing & Intellectual Properties International Journal* **2018**, *1*, 1-17, http://dx.doi.org/10.32474/DDIPIJ.2018.01.000114.
33. Romani, D.; Brandán, S.A. Effect of the side chain on the properties from cidofovir to brincidofovir, an experimental antiviral drug against to Ebola virus disease. *Arabian Journal of Chemistry* **2019**, *12*, 2959–2972, http://dx.doi.org/10.1016/j.arabjc.2015.06.030.
34. Brandán, S.A. Understanding the potency of heroin against to morphine and cocaine. *International Journal of Science and Research Methodology*, **2018**, *12*, 97-140.
35. Rudyk, R.A.; Checa, M.A.; Catalán, C.A.N.; Brandán, S.A. Structural, FT-IR, FT-Raman and ECD spectroscopic studies of free base, cationic and hydrobromide species of scopolamine alkaloid. *J. Mol. Struct*. **2019**, *1180*, 603-617, https://doi.org/10.1016/j.molstruc.2018.12.040
36. Meldrum, B.S. Update on the mechanism of action of antiepileptic drugs. *Epilepsia* **1996**, *37*, S4–S11.
37. Manzur, M.E.; Brandán, S.A. S(-) and R(+) Species Derived from Antihistaminic Promethazine Agent: Structural and Vibrational Studies. *Heliyon* **2019**, *5*, https://doi.org/10.1016/j.heliyon.2019.e02322.
38. Brandán, S.A. Structural and Vibrational Studies of Equilenin, Equilin and Estrone Steroids. *Biointerface Research in Applied Chemistry* **2019**, *9*, 4502-4516, https://doi.org/10.33263/BRIAC96.502516.
39. O' Boyle, N.M.; Tenderholt, A.L.; Langner, K.M. GaussSum 3.0 program. *J. Comp. Chem*. **2008**, *29*, 839-845.

Supplementary files

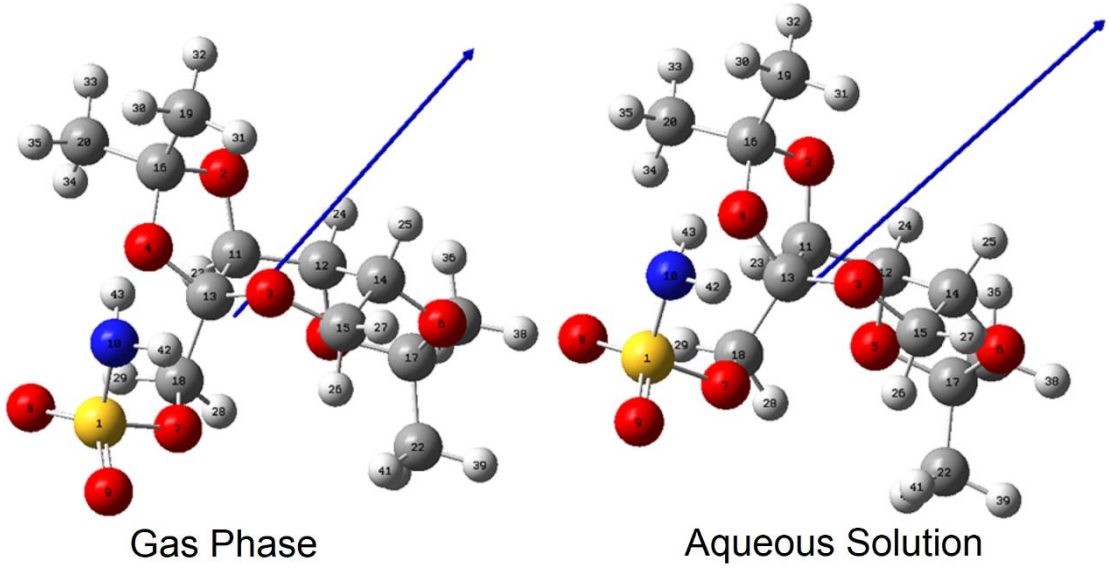

Figure S1. Orientations and directions of dipole moment vectors predicted for topiramate in both media by using the B3LYP/6-311++G** level of theory

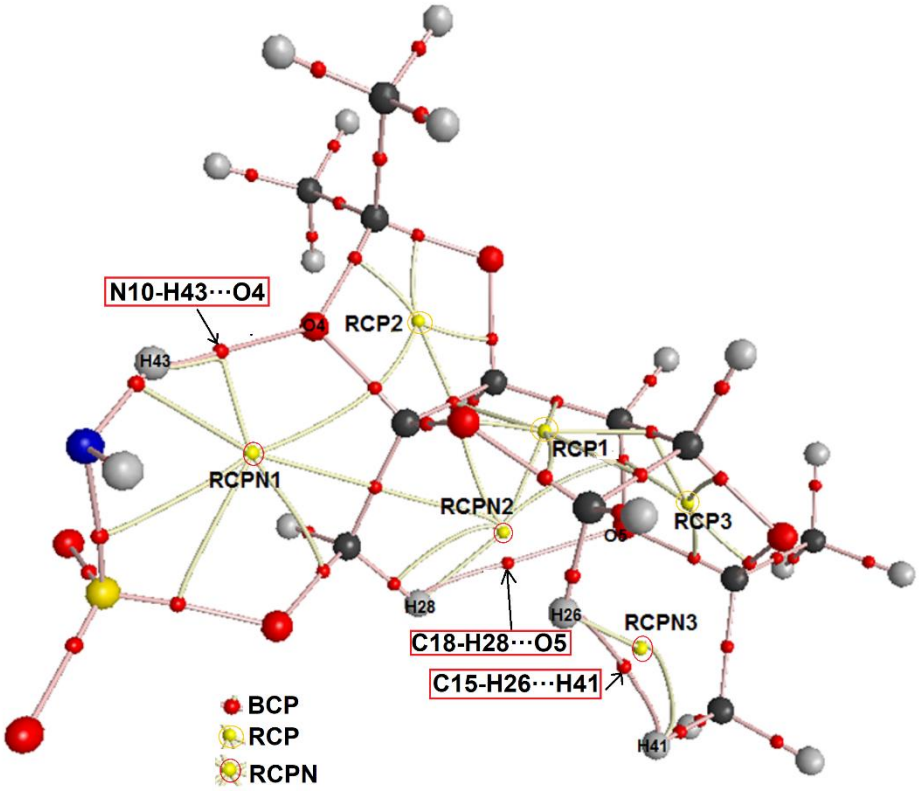

Figure S2. Molecular graphics of topiramate in gas phase showing their three H bonds interactions, three new RCPN and three RCPs by using the B3LYP/6-311++G** method.

Table S1. Mulliken, Merz-Kollman and NPA charges (a.u.), molecular electrostatic potentials (MEP) (a.u.) and bond orders, expressed as Wiberg indexes of topiramate in gas phase and aqueous solution by using B3LYP/6-311++g(d,p) calculations.

Topiramate										
	GAS					PCM				
Atoms	MK	Mulliken	NPA	MEP	BO	MK	Mulliken	NPA	MEP	BO
1 S	1,1873	0,4537	2,3709	-58,9862	4,2805	1,2095	0,4559	2,3860	-58,9885	4,2841
2 O	-0,6749	0,1340	-0,6118	-22,3332	1,9999	-0,6336	0,1189	-0,6086	-22,3314	2,0013
3 O	-0,3563	0,1039	-0,6170	-22,3358	2,0136	-0,3728	0,0027	-0,6069	-22,3408	2,0152
4 O	-0,4780	0,0982	-0,6409	-22,3269	2,0143	-0,4826	0,0427	-0,6508	-22,3275	2,0116
5 O	-0,5645	0,1269	-0,6225	-22,3355	1,9912	-0,6098	0,1300	-0,6237	-22,3368	1,9865
6 O	-0,6202	0,0680	-0,6190	-22,3453	1,9873	-0,6150	0,0517	-0,6227	-22,3473	1,9790
7 O	-0,4034	0,0124	-0,7370	-22,3182	1,8957	-0,4192	-0,0312	-0,7421	-22,3177	1,8982
8 O	-0,4858	-0,2251	-0,8889	-22,3694	1,6898	-0,5088	-0,2523	-0,9018	-22,3772	1,6687
9 O	-0,4976	-0,0949	-0,8719	-22,3730	1,7055	-0,5164	-0,1375	-0,8849	-22,3828	1,6814
10 N	-0,8528	-0,5071	-1,0126	-18,3631	2,7704	-0,8455	-0,5364	-1,0169	-18,3611	2,7736
11 C	0.4848	-0.1045	0.0868	-14.6825	3.8816	0.2683	-0.1139	0.0861	-14.6810	3.8801
12 C	0.0112	-0.3010	0.0977	-14.6882	3.8778	0.1444	-0.3580	0.0990	-14.6876	3.8791
13 C	-0.0558	-0.7853	0.5505	-14.6308	3.8643	0.0136	-0.0491	0.5493	-14.6296	3.8702
14 C	0.3559	-0.3261	0.0928	-14.6957	3.8783	0.2169	-0.3110	0.0933	-14.6968	3.8782
15 C	0.0570	-0.0443	-0.0498	-14.7049	3.8277	0.1658	-0.0644	-0.0475	-14.7061	3.8309
16 C	1.0252	-0.8750	0.6002	-14.6365	3.8172	1.0352	-0.9306	0.6029	-14.6346	3.8178
17 C	0.9551	-0.8033	0.5907	-14.6442	3.8308	0.9798	-0.8244	0.5936	-14.6445	3.8310
18 C	0.1070	-0.4172	-0.0801	-14.6908	3.8116	0.1569	-0.7519	-0.0641	-14.6886	3.8081
19 C	-0.5031	-0.1879	-0.6058	-14.7661	3.8868	-0.5556	-0.1718	-0.6008	-14.7630	3.8858
20 C	-0.5534	-0.2010	-0.6028	-14.7648	3.8896	-0.5450	-0.1920	-0.6089	-14.7631	3.8896
21 C	-0.5203	-0.2614	-0.6079	-14.7683	3.8928	-0.4367	-0.2458	-0.6083	-14.7684	3.8925
22 C	-0.6958	-0.1166	-0.5981	-14.7673	3.8906	-0.6988	-0.0923	-0.5984	-14.7673	3.8909
23 H	0.0307	0.2331	0.1951	-1.0825	0.9656	0.0798	0.2421	0.1955	-1.0806	0.9656
24 H	0.1027	0.2250	0.1946	-1.0908	0.9659	0.1016	0.2207	0.1948	-1.0908	0.9659
25 H	0.0315	0.2302	0.1994	-1.0932	0.9631	0.0649	0.2303	0.2005	-1.0934	0.9626
26 H	0.0729	0.2121	0.1777	-1.0968	0.9725	0.0453	0.2312	0.1719	-1.0961	0.9744
27 H	0.0860	0.2078	0.2007	-1.0937	0.9619	0.0707	0.2094	0.2029	-1.0945	0.9610
28 H	0.1022	0.2007	0.2157	-1.0787	0.9566	0.1069	0.2076	0.2102	-1.0758	0.9588
29 H	0.0899	0.3038	0.2248	-1.0803	0.9522	0.0678	0.2724	0.2202	-1.0782	0.9543
30 H	0.1119	0.1600	0.2096	-1.0983	0.9579	0.1268	0.1624	0.2106	-1.0944	0.9575
31 H	0.1375	0.1986	0.2235	-1.1043	0.9530	0.1557	0.1845	0.2242	-1.1011	0.9526
32 H	0.1278	0.1747	0.2146	-1.0985	0.9557	0.1424	0.1741	0.2161	-1.0952	0.9550
33 H	0.1312	0.1780	0.2130	-1.0987	0.9564	0.1250	0.1785	0.2134	-1.0965	0.9564
34 H	0.1478	0.1460	0.2114	-1.1006	0.9576	0.1536	0.1406	0.2105	-1.0969	0.9579
35 H	0.1314	0.1742	0.2169	-1.0987	0.9548	0.1296	0.1897	0.2184	-1.0964	0.9542
36 H	0.1295	0.1373	0.2067	-1.1026	0.9596	0.1042	0.1398	0.2079	-1.1021	0.9591
37 H	0.1288	0.1684	0.2097	-1.1027	0.9579	0.1064	0.1679	0.2101	-1.1022	0.9578
38 H	0.1380	0.1770	0.2155	-1.1020	0.9554	0.1132	0.1760	0.2156	-1.1015	0.9554
39 H	0.1761	0.1762	0.2156	-1.1011	0.9552	0.1741	0.1760	0.2157	-1.1005	0.9552
40 H	0.1766	0.1705	0.2132	-1.1010	0.9563	0.1766	0.1722	0.2134	-1.1003	0.9562
41 H	0.1950	0.1424	0.2098	-1.1038	0.9590	0.1900	0.1250	0.2092	-1.1028	0.9594
42 H	0.4115	0.3001	0.3949	-1.0018	0.8472	0.4054	0.3204	0.3983	-0.9979	0.8443
43 H	0.4185	0.3369	0.4137	-1.0034	0.8331	0.4085	0.3394	0.4164	-1.0003	0.8303

Table S2. Main delocalization energies (in kJ/mol) of topiramate in gas phase and aqueous solution by using B3LYP/6-311++g(d,p) calculations.

Delocalization	B3LYP/6-311++g(d,p)[a]	
	Topiramate	
	Gas	Water
*σS1-O7→ σ*S1-O8*		11.28
*σS1-O7→ σ*S1-O9*	11.78	12.20
*σS1-O7→ σ*S1-N10*	11.91	
*σS1-O8→ σ*S1-O7*	18.43	17.55
*σS1-N10→ σ*S1-O7*	14.96	13.62
*σ C11-H23→σ*O3-C13*	17.51	16.21
*σ C15-H27→σ*O3-C13*	13.79	13.20
*σ C18-H28→σ*S1-O7*	14.92	13.21
*σ C18-H28→σ*O4-C13*	19.31	19.52
*σ C18-H29→σ*O3-C13*	19.01	20.39
*σ C19-H30→σ*O2-C16*	20.39	21.69
*σ C19-H31→σ*C16-C2*		4.11
*σ C19-H32→σ*O4-C16*	23.07	23.82
*σ C20-H33→σ*O4-C16*	21.15	22.53
*σ C20-H34→σ*C16-C19*	16.72	16.46
*σ C20-H35→σ*O2-C16*	22.07	22.94
*σ C21-H36→σ*C17-C22*	15.80	16.26

Delocalization	B3LYP/6-311++g(d,p)[a]	
	Topiramate	
	Gas	Water
*σ C31-H37→σ*O6-C17*	20.27	21.44
*σ C21-H38→σ*O5-C17*	21.94	22.69
*σ C22-H39→σ*O5-C17*	20.77	21.40
*σ C22-H40→σ*O6-C17*	22.19	23.03
*σ C22-H41→σ*C17-C21*	16.42	16.80
$\Delta E_{\sigma\rightarrow\sigma^*}$	**362.41**	**370.35**
*LP(1)O2→σ*O4-C16*	13.41	17.89
*LP(2)O2→σ*C11-C13*		12.74
*LP(2)O2→σ*C11-H23*	33.27	30.09
*LP(2)O2→σ*C16-C19*	12.12	
*LP(2)O2→σ*C16-C20*	24.87	25.12
*LP(1)O3→σ*O4-C13*	17.13	16.30
*LP(2)O3→σ*C11-C13*	21.27	19.56
*LP(2)O3→σ*C13-C18*	33.02	32.26
*LP(2)O3→σ*C14-C15*	21.81	20.56
*LP(2)O3→σ*C15-H26*	23.28	22.48
*LP(1)O4→σ*O2-C16*	12.58	13.20
*LP(1)O4→σ*N10-H43*		14.88
*LP(2)O4→σ*O3-C13*	56.47	56.30
*LP(2)O4→σ*C16-C19*	19.93	15.42
*LP(2)O4→σ*C16-C20*	12.33	17.43
*LP(2)O5→σ*O6-C17*		14.96
*LP(2)O5→σ*C12-C14*	11.87	11.53
*LP(2)O5→σ*C12-H24*	31.68	30.51
*LP(2)O5→σ*C17-C21*	26.20	25.28
*LP(1)O6→σ*O5-C17*	15.80	14.33
*LP(2)O6→σ*C14-C15*	29.17	27.46
*LP(2)O6→σ*C14-H25*	12.45	11.91
*LP(2)O6→σ*C17-C21*	20.94	19.68
*LP(2)O6→σ*C17-C22*	18.68	18.05
*LP(1)O7→σ*S1-O8*		12.24
*LP(2)O7→σ*S1-N10*	31.72	36.49
*LP(2)O7→σ*C13-C18*	28.50	23.53
*LP(2)O8→σ*S1-O7*	22.69	42.21
*LP(2)O8→σ*S1-O9*	30.05	16.42
*LP(2)O8→σ*S1-N10*	90.20	85.98
*LP(3)O8→σ*S1-O7*	113.11	86.14
*LP(3)O8→σ*S1-O9*	52.04	64.53
*LP(2)O9→σ*S1-O7*	19.72	23.53
*LP(2)O9→σ*S1-O8*	33.23	28.50
*LP(2)O9→σ*S1-N10*	92.75	88.69
*LP(3)O9→σ*S1-O7*	104.41	93.46
*LP(3)O9→σ*S1-O8*	54.38	56.84
*LP(1)N10→σ*S1-O7*	46.35	51.79
$\Delta E_{LP\rightarrow\sigma^*}$	**1262.02**	**1269.15**
*σ*S1-O7→σ*S1-N10*	12.87	21.81
*σ*S1-O7→σ*O7-C18*	18.81	27.50
$\Delta E_{\sigma^*\rightarrow\sigma^*}$	**31.68**	**49.31**
ΔE_{TOTAL}	**1656.11**	**1688.81**

[a]This work

Table S3. Analysis of the Bond Critical Points (BCPs) and Ring critical point (RCPs) for topiramate in gas phase by using the B3LYP/6-311++g(d,p) method.

B3LYP/6-311++G(D,P) Method									
GAS PHASE									
Parameter[#]	H43-O4	H28-O5	H26-H41	RCPN1	RCPN2	RCPN3	RCP1	RCP2	RCP3
ρ(r)	0.0202	0.0065	0.0051	0.0068	0.0061	0.0050	0.0194	0.0436	0.0440
∇2ρ(r)	0.0728	0.0212	0.0164	0.0328	0.0256	0.0192	0.1192	0.3004	0.2968
λ1	-0.0245	-0.0051	-0.0039	-0.0026	-0.0036	-0.0029	-0.0158	-0.0472	-0.0466
λ2	-0.0242	-0.0039	-0.0022	0.0150	0.0060	0.0029	0.0644	0.1613	0.1643
λ3	0.1219	0.0307	0.0228	0.0206	0.0235	0.0192	0.0706	0.1865	0.1794
|λ1|/λ3	0.2009	0.1661	0.1710	0.1262	0.1531	0.1510	0.2237	0.2530	0.2597
Distances (Å)	2.065	2.733	2.406						

[#]In a.u.

Table S4. Analysis of the Bond Critical Points (BCPs) and Ring critical point (RCPs) for topiramate in aqueous solution by using the B3LYP/6-311++g(d,p) method.

B3LYP/6-311++G(D,P) Method							
AQUEOUS SOLUTION							
Parameter[#]	H43-O4	H26-H41	RCPN1	RCPN2	RCP1	RCP2	RCP3
ρ(r)	0.0203	0.0052	0.0075	0.0051	0.0191	0.0430	0.0431
$\nabla^2\rho(r)$	0.0744	0.0164	0.0340	0.0192	0.1172	0.2968	0.2924
λ1	-0.0244	-0.0040	-0.0034	-0.0029	-0.0156	-0.0460	-0.0455
λ2	-0.0237	-0.0024	0.0097	0.0032	0.0633	0.1566	0.1588
λ3	0.1230	0.0231	0.0281	0.0192	0.0698	0.1863	0.1793
|λ1|/λ3	0.1983	0.1731	0.1209	0.1510	0.2234	0.2469	0.2537
Distances (Å)	2.067	2.397					

[#]In a.u

Table S5. Frontier molecular HOMO and LUMO orbitals, gap values and chemical potential (μ), electronegativity (χ), global hardness (η), global softness (S), global electrophilicity index (ω) and nucleophilicity indexes (E) descriptors (in eV) of topiramate in gas phase and aqueous solution by using the B3LYP/6-311++G(D,P) level of theory.

B3LYP/6-311++G**			B3LYP/6-31G*			
Topiramate[a]			Scopolamine[b]		Promethazine[c]	
Orbital	Gas	PCM	Gas	PCM	Gas	PCM
HOMO	-7.5114	-7.5024	-5.7650	-5.8338	-5.0096	-5.0559
LUMO	-0.5680	-0.5708	-0.3646	-0.3580	-0.2939	-0.2857
|GAP|	6.9434	6.9316	5.4004	5.4758	4.7157	4.7702
Descriptors						
μ	-3.4717	-3.4658	-2.7002	-2.7379	-2.3579	-2.3851
χ	-4.0397	-4.0366	-3.0648	-3.0959	-2.6518	-2.6708
η	3.4717	3.4658	2.7002	2.7379	2.3579	2.3851
S	0.1440	0.1443	0.1852	0.1826	0.2121	0.2096
ω	2.3503	2.3507	1.7393	1.7504	1.4911	1.4954
E	-14.025	-13.990	-8.2756	-8.4763	-6.2524	-6.3701

[a]This work, [b]From Ref [35], [c]From Ref [37]

χ = - [E(LUMO)- E(HOMO)]/2 ; μ = [E(LUMO) + E(HOMO)]/2; η = [E(LUMO) - E(HOMO)]/2; S = ½η; $\omega = \mu^2/2\eta$; $E=\mu*\eta$

Table S6. Observed and calculated ^{1}H chemical shifts (δ in ppm) for Topiramate in different media by using the B3LYP/6-311++G(D,P) method.

Topiramate[a]			Exp[b]
H atom	Gas	Water	
23-H	3.90	3.94	4.33
24-H	4.40	4.33	4.65
25-H	4.17	4.14	4.28
26-H	3.46	3.31	3.82
27-H	3.74	3.71	3.94
28-H	4.53	4.46	4.37
29-H	4.33	4.16	4.27
30-H	1.39	1.35	1.19
31-H	1.64	1.49	1.19
32-H	1.46	1.46	1.19
33-H	1.28	1.14	1.19
34-H	1.39	1.45	1.19
35-H	1.53	1.41	1.19
36-H	1.43	1.36	1.19
37-H	1.14	1.07	1.19
38-H	1.33	1.28	1.19
39-H	1.53	1.47	1.19
40-H	1.62	1.55	1.19
41-H	1.25	1.17	1.19
42-H	3.82	3.95	4.92

Topiramate[a]			Exp[b]
H atom	Gas	Water	
43-H	6.06	5.91	4.92
RMSD	**0.42**	**0.38**	

[a]This work GIAO/B3LYP/6-311++G(D,P) Ref. to TMS, [b]From Ref [7]

Table S7. Observed and calculated ^{13}C chemical shifts (δ in ppm) for topiramate in different media by using the B3LYP/6-311++G(D,P) method.

Topiramate[a]			Exp[b]
C atoms	Gas	Water	
11-C	78.95	79.37	70.9
12-C	77.80	77.63	70.9
13-C	106.32	106.66	101.3
14-C	72.27	72.57	70.0
15-C	66.62	66.87	59.7
16-C	119.34	119.84	120.1
17-C	116.77	117.90	105.3
18-C	68.50	71.35	70.0
19-C	28.32	27.00	28.1
20-C	26.67	24.54	27.2
21-C	25.58	25.13	25.9
22-C	29.14	28.78	26.8
RMSD	**4.69**	**5.01**	

[a]This work GIAO/B3LYP/6-311++G(D,P) Ref. to TMS, [b]From Ref [7]